Time-Resolved Investigation of Energy Transfer in Carbon Nanotube-Porphyrins Compounds.

ARTICLE *in* THE JOURNAL OF PHYSICAL CHEMISTRY C · DECEMBER 2011

Impact Factor: 4.77 · DOI: 10.1021/jp207267e

9 AUTHORS, INCLUDING:

Cyrielle Roquelet
ArcelorMittal
47 PUBLICATIONS **192** CITATIONS
SEE PROFILE

Thierry Michel
Université de Montpellier
36 PUBLICATIONS **638** CITATIONS
SEE PROFILE

Jean-Sébastien Lauret
Ecole normale supérieure de Cachan
144 PUBLICATIONS **1,592** CITATIONS
SEE PROFILE

Christophe Voisin
Ecole Normale Supérieure de Paris
174 PUBLICATIONS **2,744** CITATIONS
SEE PROFILE

Time-resolved investigation of excitation energy transfer in carbon nanotube-porphyrin compounds

Damien Garrot[1], Benjamin Langlois[2], Cyrielle Roquelet[1], Thierry Michel[2],* Philippe Roussignol[2], Claude Delalande[2], Emmanuelle Deleporte[1], Jean-Sébastien Lauret[1], and Christophe Voisin[2]†

[1] *Laboratoire de Photonique Quantique et Moléculaire, Institut d'Alembert, CNRS, ENS Cachan, 94235 Cachan, France and*

[2] *Laboratoire Pierre Aigrain, Ecole Normale Supérieure, Université Paris Diderot, UPMC, CNRS UMR8551, 24 rue Lhomond, 75005 Paris, France*

(Dated: September 5, 2011)

Single-wall carbon nanotubes non-covalently functionalized with porphyrin molecules have proven to be a very promising light harvesting system either for energy or charge transfer. In this paper we investigate the dynamics of this coupling at a sub-picosecond time-scale, by means of transient absorption spectroscopy. We show that the ground state recovery time of the porphyrin is reduced by several orders of magnitude compared to the case of pristine porphyrin. Concomitantly, a strong bleaching signal is observed on the optical resonances of the nanotubes showing an ultrafast population buildup upon excitation of the porphyrin. We conclude that the energy transfer occurs on a time-scale shorter than 100 fs. Two-color measurements show that higher excited states of the nanotubes are populated on the same time-scale raising the point of the transfer mechanism. We briefly discuss two possible mechanisms.

I. INTRODUCTION

Single Wall Carbon Nanotubes (SWNTs) are well known for their high carrier mobility and strong resonant optical absorption that make them attractive for nanoscale optoelectronic devices [1]. However in this perspective several issues still need to be addressed. Current synthesis methods produce a mix of carbon nanotubes with a wide variety of structures and therefore with electronic transitions spreading over a broad energy range. Another important issue is related to the single-atomic-layer structure of SWNTs that makes them very sensitive to their environment. When uncontrolled this interaction with the environment can be penalizing, leading to unintentional and drastic changes in the transport or optical properties of the tube [2, 3]. On the other hand, this interaction can be used to intentionally tune the opto-electronic properties of the device by means of functionalization with appropriate molecules. The goal is to combine the unique properties of nanotubes with the wide tunability of organic molecules properties.

Among those molecules, porphyrins are well known for their key role in many important biological processes, such as oxygen transport in blood or such as light harvesting units in photosynthetic centers. Their widely delocalized π electron system gives rise to strong absorption in the visible that is already used in dye sensitized hybrid solar cells [4]. Porphyrins have also been combined with different molecules such as fullerenes and carbon nanotubes to form electron donor/acceptor systems for artificial photosynthetic devices [5, 6].

This large π-electronic system of porphyrins also allows them to link non covalently to carbon nanotubes through π-stacking interaction [7, 8]. In contrast to covalent functionalization, this mild interaction preserves most of the intrinsic properties of the nanotubes, as shown by photoluminescence measurements, but still leads to a strong enough coupling so to induce new functionalities. In particular it was shown recently that efficient Excitation Energy Transfer (EET) can occur in such systems [9, 10]. The very high quantum yield reported in this system [11] suggests that the EET mechanism must occur on an ultrafast time-scale.

In this paper we present a detailed investigation of EET in SWNT/porphyrin compounds at room temperature with a particular emphasis on the dynamics at a sub-picosecond time-scale. We conduct a careful comparison of the dynamics in such compounds and in two reference samples made of the pristine materials.

The relaxation dynamics of the excited states of free base Tetra Phenyl Porphyrin (TPP) has been under investigation for many years [12–15]. Baskin et *al* [16] have studied the ultrafast relaxation of TPP in benzene and have observed a fast population relaxation subsequent to absorption of a laser pulse in the Soret band (ground state to B state transition, see inset of Fig. 1). The population decay from the B electronic state to the Q_x states occurs in less than 100 fs. This rapid flow of population into vibrationally excited levels of Q_x is followed by vibrational energy redistribution on a longer timescale of 10-20 ps. A lifetime of 12 ns was reported from time-resolved photoluminescence of the Q_x band [17]. The dominant relaxation path of Q_x is inter-system crossing to the triplet state T [18].

In SWNTs, electron - hole pairs are strongly coupled due to the reduced screening of the Coulomb interaction in one dimensional systems and form strongly bound excitons [19–21]. Those excitons have binding energies on the order of several hundreds of meV and are responsible for most of the optical properties of semi-conducting

* now at Laboratoire Coulomb, Université de Montpellier

† christophe.voisin@lpa.ens.fr

SWNTs. The dynamics of excitons in SWNTs has been investigated by several groups [22–24] and the influence of the environment on this dynamics turns out to be critical [25–27].

In contrast, the electron and energy relaxation dynamics in SWNTs non-covalently functionalized by TPP molecules is poorly documented to date. In this study, we show that in this system, the relaxation dynamics of the porphyrin is dramatically modified and that EET occurs on a sub-picosecond time-scale. Two-color broad band pump-probe measurements at room temperature allow us to track the population dynamics in the subunits of the complex and draw conclusions about the main lines of the energy transfer mechanism. We further investigate how the internal dynamics of the nanotubes is affected and address the question of a possible chirality dependence of the transfer yield. Finally we compare our results to two possible microscopic EET mechanisms.

II. SAMPLES AND EXPERIMENTAL PROCEDURES

A. Linear optical properties : absorption

Fig. 1(a) displays the Optical Absorption Spectrum (OAS) and Photo Luminescence (PL) spectrum of a water suspension of TPP embedded in micelles of sodium cholate (SC). The absorption shows the so-called Soret band at 420 nm and four weaker Q bands in the 500-700 nm region. The Q bands are degenerate in the D_{4h} symmetry of metallo-porphyrins but split in two electronic components Q_x and Q_y in the case of free base TPP. Four vibronic peaks at 516 nm, 549 nm, 589 nm, 645 nm, correspond to this Q band and were assigned to $Q_y(1,0)$, $Q_y(0,0)$, $Q_x(1,0)$, $Q_x(0,0)$ (numbers in parentheses indicate the number of quanta of the dominant Franck-Condon active vibrational mode in the upper and lower electronic states of the transition, respectively) [16]. The lowest triplet state T_1 lies approximately 0.5 eV below the Q_x state.

The nanotubes used in this study are synthesized by the CoMoCAT process and produced by SouthWest Nanotechnologies (SG65). The mean diameter of these tubes is about 0.8 nm. SWNTs are first processed in water with surfactant and ultrasonic waves in order to split the bundles into individual nanotubes encased in micelles. Fig. 1(b) shows the OAS of pristine SWNTs in a SC micelle suspension. The OAS of SWNTs consists in a group of lines near 1000 nm corresponding to the so-called S_{11} (lowest) transitions in semi-conducting nanotubes. Each line in this group stems from a given (n, m) chiral species. Additional lines in the 400-700 nm range stem from S_{22} transitions superimposed to the onset of M_{11} transitions in metallic nanotubes. The background in OAS is not completely elucidated to date, but mainly stems from light scattering, absorption from residual metallic species and residual amorphous carbon nanoparticles [28].

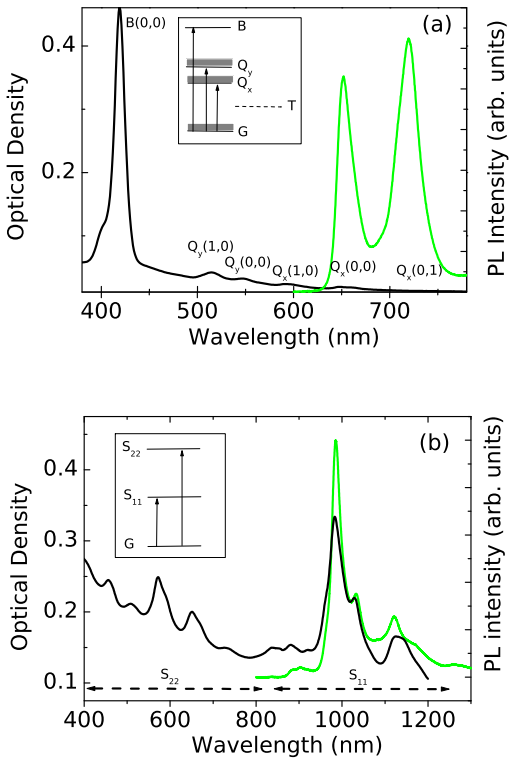

FIG. 1. (color online) Optical absorption spectrum of TPP molecules (a) and carbon nanotubes (b) (black lines) in a SC micelle suspension in a pH 8 buffer. The PL spectrum of the same suspensions excited at 532 nm is displayed in green. Insets : sketch of the energy levels.

The functionalization of SWNTs with TPP is achieved by the micelle swelling technique, as described in Ref. [29]. The sample consists in an aqueous suspension of non-covalently bound SWNT/TPP complexes embedded in SC micelles. The OAS of the SWNT/TPP suspension (Fig. 2) shows a band at 438 nm with a shoulder at 420 nm. This latter is assigned to the Soret absorption band of residual free TPP encased in micelles (in agreement with the OAS of pristine TPP) and the former (438 nm) is assigned to the Soret absorption line of TPP bound to nanotubes. This 18 nm redshift is consistent with previous observations [9, 30] and is related to a conformational change of TPP molecules when stacked on the nanotubes. The presence of these two bands shows that the suspension contains both pristine TPP molecules encased in micelles and TPP bound to nanotubes in micelles. The absorption features around 1000 nm are consistent with S_{11} absorption lines in semiconducting nanotubes. We note a 20 nm redshift compared to the reference suspension of pristine nanotubes, which we interpret as a consequence of an increased dielectric screening of excitons in nanotubes in the presence of TPP [3]. Importantly, the amplitude of the S_{11} absorption lines is almost identical in the reference sam-

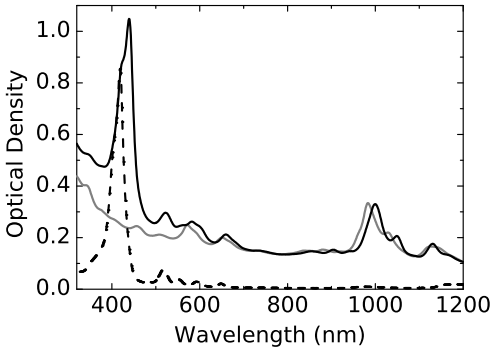

FIG. 2. Optical absorption spectra of TPP molecules (dashed line), of a reference suspension of SWNT (gray line) and of SWNT/TPP complexes (black line), all of them embedded in SC micelles in a pH 8 buffer.

ple of pristine nanotubes and in the compounds. This means that the concentration of the different species of nanotubes is almost unchanged after the functionalization step. This will allow quantitative comparisons of the transient spectra presented in the following. In the visible region, we note several absorption lines from which the contribution of the TPP Q bands and the SWNT S_{22} bands are more difficult to single out.

B. Luminescence properties and Excitation Energy Transfer

1. *Pristine materials*

The luminescence spectrum of a reference sample of porphyrin is shown in Fig. 1(a). It consists in a set of lines in the visible corresponding to the Franck-Condon transitions from the Q_x band. This luminescence is strongly enhanced when the excitation is in resonance with the Soret band [9].

Fig. 1(b) shows the luminescence properties of a reference suspension of carbon nanotubes. This luminescence spectrum consists of a set of lines in the near infrared (NIR) arising from the S_{11} excitonic transition in the different chiral species present in the sample with negligible Stokes shifts. The excitation spectrum of one of those lines (Fig. 3(a)) shows a resonance in the visible related to absorption on the S_{22} excitonic resonance. These pairs of resonances (S_{11} and S_{22}) allow the identification of the chiral species [31].

2. *Excitation Energy Transfer*

The luminescence spectrum of the SWNT/TPP compounds is characterized by a strong quenching of the luminescence of the Q bands of the porphyrin (almost 3

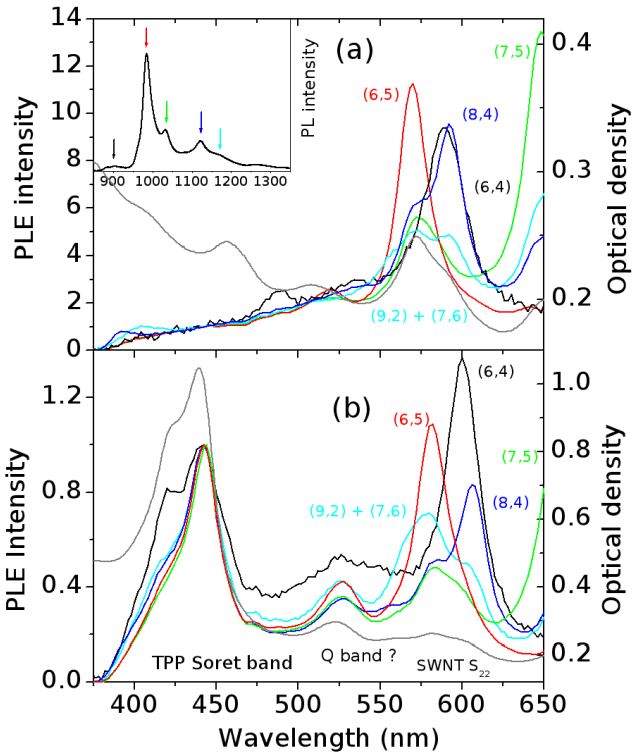

FIG. 3. (a) Normalized (at 438 nm) excitation spectra of the luminescence of a suspension of carbon nanotubes at selected wavelengths as indicated by arrows in the inset. The resonances arise from S_{22} transitions and allow the assignment of each line to a given chiral species (indicated in parentheses). Absorption spectrum of the same suspension (dashed line). Inset : NIR photoluminescence spectrum of the same suspension for an excitation wavelength of 532 nm. The luminescence arises from S_{11} excitons. (b) Normalized (at 438 nm) excitation spectra of the luminescence of a suspension of SWNT/TPP compounds at selected wavelengths. The resonances arise from S_{22} transitions and from EET upon absorption on the Soret band of the porphyrin. The numbers in parentheses indicate the most likely assignment to a chiral species of nanotubes. Absorption spectrum of the same suspension (dashed line).

orders of magnitude [11]). In contrast, the luminescence of the nanotubes is almost unchanged except for a redshift on the order of 20 nm consistent with the redshift observed in absorption. More interesting is the excitation spectrum of the compound (Fig. 3(b)) which is dramatically modified compared to the one of pristine nanotubes. In particular, we note the appearance of a strong additional resonance at 438 nm for all the chiral species. This resonance corresponds to Excitation Energy Transfer to the nanotubes upon excitation on the Soret band of the porphyrin. The EET resonance has the same magnitude as the one of intrinsic S_{22} resonances showing qualitatively a very efficient transfer yield [11]. Note that the shoulder at 420 nm in the PLE spectra (and notably in the one of (6,4) nanotubes) arises from free TPP, since the PL tail of the latter overlaps with the PL of nanotubes.

In addition, a moderate excitation line is observable at 525 nm. This line might be a direct excitation of the nanotubes through the phonon side-band of S_{22} [32]. However, this side-band is much weaker in the PLE spectrum of pristine nanotubes and its position depends on the chiral species (cf. Fig.3(a)). We rather think that this excitation line of the compound corresponds to another EET path subsequent to the excitation of TPP through a Q band [11]. This is consistent with the spectral position of the line which does not depend on the chiral species in the compound. This observation raises the point of the role of the Q states in the EET mechanism.

C. Pump-probe setup

Two different setups have been used, one for degenerate pump-probe measurements and the other for two-color measurements. The degenerate pump-probe measurement setup is based on a frequency doubled mode-locked Ti:Sapphire laser delivering 100 fs pulses at a repetition rate of 80 MHz in the 800-880 nm wavelength range.

For two-color measurements, the pump-probe setup is based on an amplified Ti:sapphire laser delivering pulses at a central wavelength of 800 nm with a duration of about 130 fs and a 250 kHz repetition rate. Part of the beam is focused in a sapphire crystal to generate a white-light continuum by self-phase modulation. About 20% of this continuum is reflected off a beam splitter for use as a broad-band probe. The rest of the amplified 800 nm beam is steered into a home-made optical parametric amplifier tunable from 445 nm to 700 nm and serves as the pump. After passing through the sample, the white probe pulse is dispersed in a spectrometer (JOBIN YVON, HR320) and is detected with an avalanche photodiode. We record the change of transmission of the sample as a function of the time delay for a given probe wavelength or as a function of the probe wavelength for a fixed time delay (transient spectrum) using standard lock-in detection techniques involving mechanical chopping of the pump beam. The chirp of the probe pulse was measured separately and is compensated in the measurements of transient spectra.

The relative polarizations of the pump and probe pulses were set parallel to each other. Note that due to the size of the SWNTs, their orientational diffusion is negligible on a picosecond time-scale. All measurements were performed at room temperature.

D. Data analysis

To be more quantitative, the relaxation dynamics are fitted to the following expression :

$$\Delta T(\tau,\lambda) = \int_{-\infty}^{+\infty} g[(t-\tau),\lambda]R(t,\lambda)dt$$

where $g(t,\lambda)$ is the instrumental response and $R(t,\lambda)$ is the sample impulse response. The latter is further expanded in terms of exponential contributions as $R(t,\lambda) = \sum_i A_i(\lambda)\exp(-t/\tau_i)$, each τ_i reflecting a specific relaxation path between a pair of electronic levels.

The correlation between the pump and probe pulses is used to set the time zero and to determine the instrumental response function. This instrumental response function (IRF) is obtained from the time profile of stimulated Raman peaks of the solvent [33]. The O-H asymmetric stretching mode is observed at $\approx 3490\ cm^{-1}$. We show that the cross-correlation function can be fitted to a Gaussian with a temporal width (FWHM) of 260 ± 10 fs (Fig. 4).

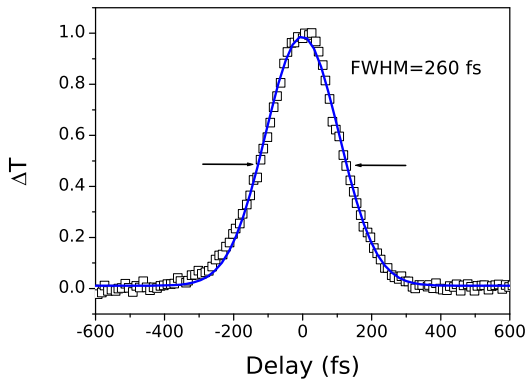

FIG. 4. Instrumental response function obtained from transient stimulated Raman gain measured in water; the signal is fitted to a Gaussian with $FWHM = 260$ fs.

Note that for dilute samples (which is a good approximation for our samples), the relative change of transmission is the exact opposite of the change of absorption ($\Delta T/T = -\Delta\alpha L$, where L is the cuvette thickness). Generally speaking, the transient response can

be described in terms of photo-bleaching (PB) (positive $\Delta T/T$) and induced absorption (IA) (negative $\Delta T/T$). The former arises from partial saturation of excitonic transitions, whereas the latter is due to absorption from populated excited states to higher excited states. Both contributions can spectrally overlap. Other nonlinear signals such as stimulated emission or stimulated Raman scattering are not observed here. As can be seen in the following PB is observed at wavelengths that correspond to absorption bands in the linear spectrum. In contrast, IA shows an almost flat spectral distribution and overlaps with PB peaks.

III. DYNAMICS : RESULTS AND DISCUSSION

A. Porphyrin dynamics : degenerate pump-probe spectroscopy

We first focus on the relaxation dynamics of TPP by comparing transient absorption spectra of the Soret band either for SWNT/TPP compounds (438 nm) or for pristine TPP encased in micelles (420 nm).

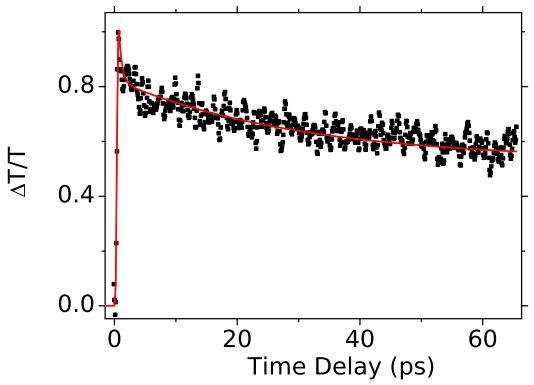

FIG. 5. Normalized $\Delta T/T$ dynamics of pristine TPP in SC micelles with pump and probe at 420 nm; solid red line : bi-exponential fit to the data. The pump fluence was 30 μJ/cm^2.

The normalized change of transmission $\Delta T/T$ is shown in Fig. 5 for both pump and probe in resonance with the Soret band of pristine TPP (420 nm). The transient transmission of TPP can be fitted to a bi-exponential with $R(t) = A_1 \exp(-t/\tau_1) + A_2 \exp(-t/\tau_2)$ with $A_1 = 0.20$, $t_1 = 0.2$ ps, $A_2 = 0.26$, $t_2 = 30$ ps. An additional slow component is required to fit the data but its decay cannot be resolved with our setup. The fast component is related to the relaxation of electrons from the B state to lower excited states (Q bands). It is on the order of 200 fs in agreement with previous studies [16]. On a longer time-scale, the absorption on the Soret band remains partially bleached since the ground state remains depopulated until the population trapped on the Q and

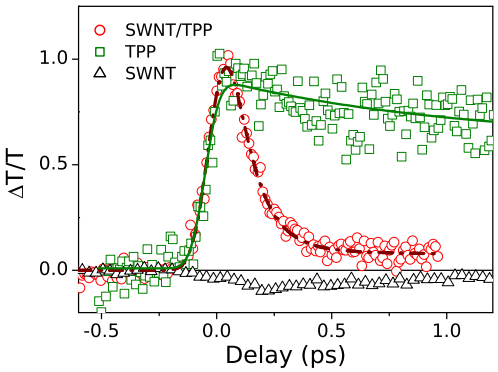

FIG. 6. Normalized $\Delta T/T$ dynamics of a micelle suspension of SWNT/TPP compounds with pump and probe at 438 nm (open circles). Dashed line : exponential fit to the data. The change of transmission in a suspension of pristine nanotubes (open triangles) and in a suspension of pristine porphyrin (open squares) is given for comparison. The normalization factor used for SWNT/TPP was applied to pristine nanotubes, which allows a direct comparison of their amplitudes since the nanotube concentration is equal in both samples (see Section II A). The pump fluence was 30 μJ/cm^2 in all cases.

triplet states relaxes. This slow component has been reported to be on the order of ≈ 12 ns [16].

In contrast, the SWNT/TPP compound shows a much faster relaxation to the ground state as shown by the fast recovery of the Soret band (Fig. 6). The residual slow component for times larger than 0.5 ps is likely the signature of residual free TPP encased in micelles. We carefully checked that the transient response of the compound at this wavelength essentially arises from the TPP subunit. Actually, SWNTs show IA when probed at this wavelength (Fig. 6) and the amplitude of the transient signal is 10 times weaker.

These results unambiguously show that the relaxation dynamics of TPP is dramatically affected by the presence of SWNTs. TPP/SWNT compounds show a full recovery of TPP subunit within one picosecond. This gives a first indication that EET between TPP and SWNT occurs on a sub-picosecond time-scale in agreement with the high quantum yield reported in the literature [11].

B. TPP to SWNT energy transfer

PLE measurements (Fig. 3(b)) show the existence of EET which results in enhanced light emission from the S_{11} transition of SWNTs when exciting the compound on the Soret band. In order to study the molecular pathway of energy transfer and its dynamics, we performed two-color pump-probe measurements reproducing the same

excitation and detection scheme as in PLE measurements : the pump is tuned in resonance with the Soret band of the compound whereas the probe is chosen in the NIR in resonance with the S_{11} transitions of SWNTs. Due to experimental constrains we were not able to use a pump wavelength strictly in resonance with Soret band of the compound. However, by selecting a pump wavelength at 445 nm we performed a fairly selective excitation of the compound (through the Soret resonance of the TPP subunit), whereas a pump wavelength of 400 nm allows a fairly selective excitation of free porphyrin (see absorption spectra in Fig. 2)

1. *Transient response of S_{11} excitons*

a. Dynamics

We first focused on the electron dynamics in the compound by tracking the population build-up on the S_{11} excitonic level of SWNTs upon excitation on the Soret band of the TPP. Figure 7(a) shows the dynamics of $\Delta T/T$ of compounds made of (6,5) nanotubes. For comparison, we show the dynamics of the same excitonic level for pristine (6,5) nanotubes. In both cases, the pump is kept at 445 nm. The most striking difference is an increase by approximately a factor of 3 of the signal amplitude for the compound compared to pristine SWNTs (for equal SWNT concentration). This roughly means that for equal pump power density the population induced on S_{11} excitonic levels is enhanced by a factor of 3 when using the TPP subunit as light-harvesting system for populating the nanotube. This observation is consistent with PLE measurements : an increase of the PL intensity by a factor of 3 to 5 is found when exciting SWNT/TPP at 438 nm compared to the PL intensity of pristine SWNTs excited at the same wavelength.

The normalized $\Delta T/T$ (Fig. 7(b)) allows us to compare the recombination dynamics of S_{11} excitons in SWNTs and in SWNT/TPP compounds. It turns out that the kinetics are nearly identical. The rise time is limited by the pulse duration and is identical for both samples. For SWNTs it is well known that the inter-subband recombination occurs on a very fast time-scale (on the order of a few tens of fs [22, 34]), which is consistent with the absence of rise-time in the transient of SWNTs. For the compound, this absence of rise-time means that we cannot resolve the excitonic population build-up and therefore that the EET also occurs on a time-scale on the order of 100 fs or less. Note that our time resolution in the two-color configuration is twice the one of the degenerate one, which may explain why we can resolve the ultra-fast decay of the porphyrin and not the population build-up in the nanotubes.

We used a bi-exponential response $R(t,\lambda) = A_1(\lambda)\exp(-t/\tau_1) + A_2(\lambda)\exp(-t/\tau_2)$ in order to fit this recombination dynamics. The fitting parameter are reported on the table I.

The recombination occurs on a ten picosecond time-scale and is very similar for both samples. We note a slight increase of the overall decay rate for the compounds but this minor acceleration of the decay is weak compared to the drastic increase of the recombination rate observed for the TPP (see Sec. III A). This is consistent with the fact that the compounds stability relies on weak $\pi-\pi$ interactions which hardly perturb the intrinsic properties of nanotubes by avoiding the creation of deep defects along the structure. Therefore, once an exciton is generated in a nanotube its further relaxation hardly depends on whether the tube is surrounded by TPP molecules or not.

b. Transient absorption spectra

In order to compare the transient response of the

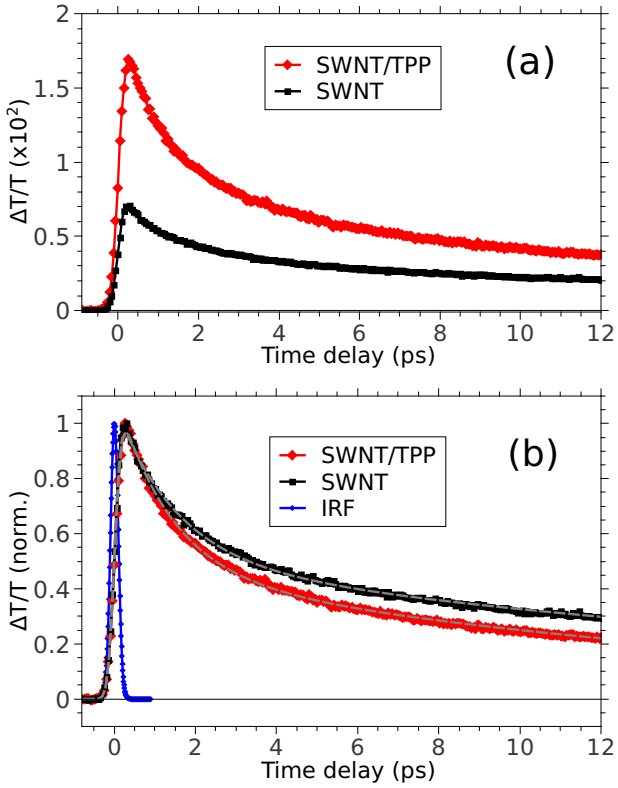

FIG. 7. $\Delta T/T$ (a) and normalized $\Delta T/T$ (b) dynamics of SWNT and SWNT/TPP suspensions excited at 445 nm and probed in resonance with S_{11} transition of (6,5) carbon nanotubes. (λ_{pr}=985 nm for SWNTs (black squares) and λ_{pr}=1005 nm for SWNT/TPP (red diamonds)) Dashed line : Bi-exponential fit of the SWNT/TPP signal. The pump fluence was 300 μJ/cm^2. Blue line : IRF.

	A_1	A_2	τ_1	τ_2
SWNT/TPP	0.3	0.25	1.3 ± 0.1ps	∼16 ps
SWNT	0.3	0.2	1.6 ± 0.1ps	∼20 ps

TABLE I. Fitting parameters of normalized $\Delta T/T$ dynamics of SWNT/TPP pumped at 445 nm and probed in resonance with S_{11} transition of the (6,5) nanotubes.

different chiral species present in the sample, we recorded transient spectra for which the pump-probe time-delay is kept constant and the wavelength of the probe is scanned in the NIR range. Again, the pump wavelength is kept at 445 nm, in resonance with the Soret band of the SWNT/TPP compound. Figure 8(b) shows the transient response ($\Delta T/T$) in the near infrared region between 870 nm and 1070 nm of SWNT/TPP compounds at several time delays (0.2 ps, 2 ps, 4 ps and 6 ps). For comparison the transient response of pristine nanotubes excited at the same wavelength is shown in Figure 8(a). Note that the reference TPP sample does not show any significant signal in this wavelength range.

We observe PB peaks for each absorption band in the linear spectrum, meaning that a sizable S_{11} exciton population is induced in all chiral species upon excitation of the porphyrin. Furthermore, we checked the transient signal is proportional to the linear absorption. If one assumes that the latter is a fair estimate of the relative abundance of each chiral species, this shows that EET is non specific. Therefore non-covalent functionalization of SWNTs with porphyrins provides a convenient way for exciting uniformly all the chiral species of a sample at one single wavelength, which is an interesting property for opto-electronic applications.

In brief, this transient spectrum shows that the population buildup on SWNT states and thus EET occur on a subpicosecond time scale. This transfer is followed by recombination with a dynamics comparable to the one observed in pristine SWNTs. In addition, all the nanotube species present in the sample display uniform EET from TPP.

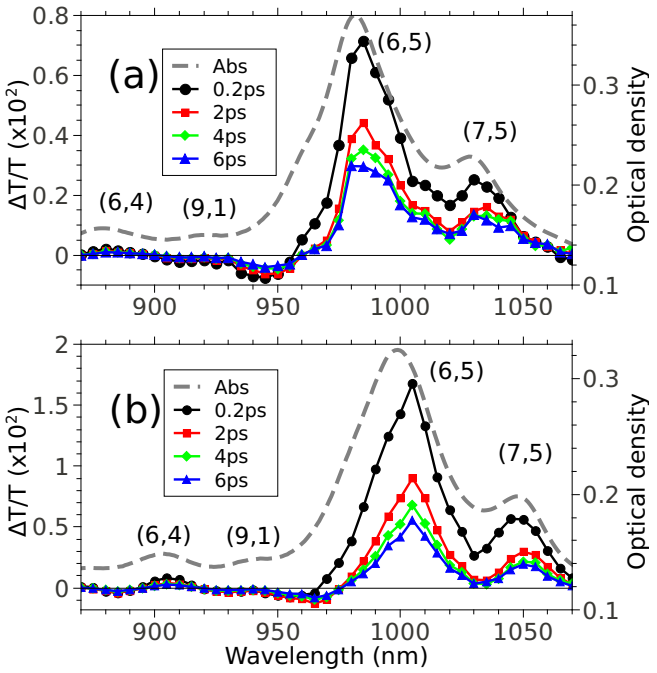

FIG. 8. Transient absorption spectra of (a) SWNTs and (b) SWNT/TPP pumped at 445 nm for several pump-probe delays (0.2, 2, 4 and 6 ps). Dashed line : linear absorption spectra. The pump fluence is 300 μJ/cm^2. The majority chiral species are indicated in parentheses.

2. *Intermediate states dynamics*

The spectral region between 500 and 720 nm allows to probe the dynamics of intermediates states of the system, namely the Q bands of the TPP subunit and the S_{22} excitonic transitions of the carbon nanotubes. Transient spectroscopy in this energy range gives unique information on the role of these intermediate states in the EET mechanism since they cannot be assessed by linear spectroscopy.

a. *Transient absorption spectra*

Transient absorption spectra of pristine SWNT, SWNT/TPP compounds and pristine TPP were measured in this wavelength range in order to identify the electro-vibrational levels of porphyrin and nanotubes specifically involved in the EET mechanism.

Figure 9(a) shows $\Delta T/T$ of pristine SWNTs probed between 500 and 720 nm at two different time delays following excitation at 445 nm with a pump fluence density of 300 $\mu J/cm^2$. Similarly to the NIR case, PB is observed at each absorption band (S_{22} transitions) superimposed to a broad negative background (IA). The origin of this background is still debated in the literature [22, 25]. PB peaks are observed at 510 nm, 570 nm, 584 nm, 651 nm and 666 nm which corresponds to the bleaching of S_{22} excitonic resonances of the (5,4), (6,5), (6,4), (7,5) and

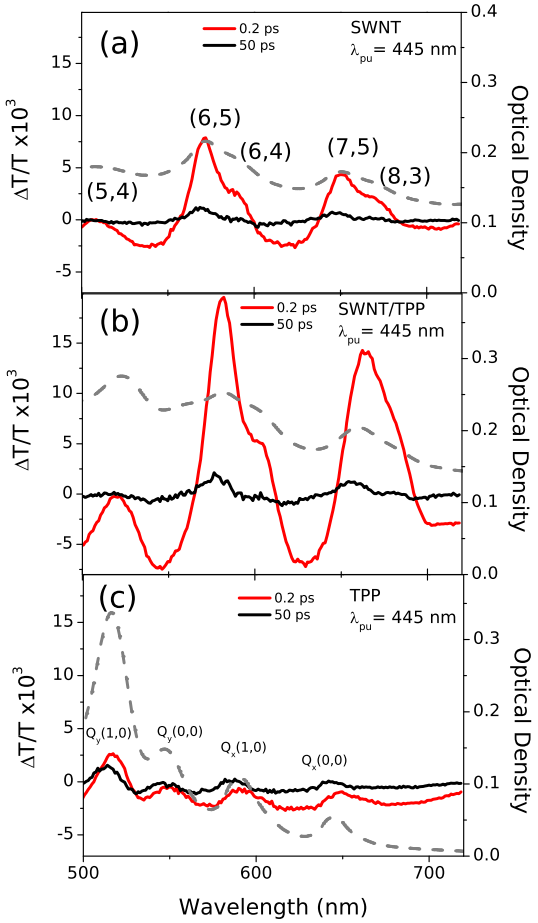

FIG. 9. Transient absorption spectra for SWNT (a), SWNT/TPP (b) and TPP (c) in SC, pumped at 445 nm at two different pump-probe delays (0.2 ps (red line) and 50 ps (black line)). The pump fluence is 300 μJ/cm^2. The dashed line is the linear absorption spectrum of the corresponding sample.

(8,3) chiral species respectively.

Figure 9(c) shows $\Delta T/T$ of pristine TPP at different time delays following excitation at 445 nm. We observe a set of PB lines corresponding to the Franck-Condon transitions of the Q bands superimposed to a broad negative background (IA). Both signals (IA and PB) have an instantaneous rise time within our temporal resolution. The spectral profile of the transient transmission does not change significantly after 600 fs except for a global decrease in amplitude and a slight blue shift. At 0.2 ps (pump-probe overlap) PB peaks are observed at 516 nm, 550 nm, 590 nm and 648 nm in good agreement with linear absorption bands (Q bands) of TPP.

Figure 9(b) shows the transient transmission spectrum of the SWNT/TPP compound for several time-delays following a resonant excitation on the Soret band at 445 nm.

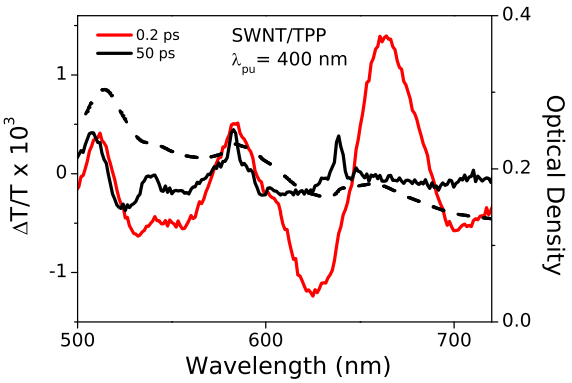

FIG. 10. Transient absorption spectra for SWNT/TPP in SC, pumped at 400 nm at two different pump-probe delays (0.2 ps (red line) and 50 ps (black line)). The pump fluence is 300 μJ/cm^2. The dashed line is the linear absorption spectrum of the corresponding sample.

This spectrum is very similar to the transient response of pristine SWNTs (Fig. 9(a)). Four PB peaks are observed at 580 nm, 598 nm and 663 nm (double peak), which are related to the corresponding S_{22} transition in the linear absorption spectrum (note the usual 20 nm redshift due to dielectric screening of the SWNT transitions by TPP [29]). The line at 518 nm is less straightforward to assign since it may arise either from (5,4) nanotubes or from one of the Q bands of the porphyrin. The amplitude of the signal is approximately twice larger than the one of pristine SWNTs pumped at the same wavelength, showing an enhanced population creation upon excitation on TPP resonances. In agreement with the observations on S_{11} transitions, this population enhancement is attributed to an efficient EET in the compound following absorption on the Soret band of the TPP subunit and no signature of any intermediate state such as transient charged states could be detected.

The main conclusion is that after excitation of the compound the spectral signature is mainly the one of nanotubes even in the very first picoseconds. This means that TPP molecules have lost their energy within this time-scale (no transient signature of TPP). In contrast, the enhanced transient response of nanotubes shows that their non equilibrium population is larger than the one observed through direct excitation, which shows the efficiency of the EET process. In other words, the hybrid states of the compound in the intermediate energy range have predominantly SWNT character. Their recombination dynamics is also essentially driven by recombination processes in SWNTs which is the fastest of the recombination paths in TPP or SWNTs.

In contrast, for off resonant pumping (400 nm), the spectrum of a suspension of SWNT/TPP compounds (Fig. 10) is more complex, whereas the transient response of the pristine materials remains qualitatively un-

changed (see supplemental material). At 0.2 ps delay, SWNT/TPP compounds show five positive peaks at 511 nm, 541 nm, 583 nm, 603 nm and 662 nm. Features at 583 nm, 603 nm and 662 nm can be attributed to the spectral response of SWNTs from qualitative comparison with Fig. 9(a). Note however that the amplitude of the signal is roughly 10 times lower than for resonant excitation. The peak at 511 nm can be attributed to the $Q_y(1,0)$ transition of TPP by comparison with Fig. 9(c). The origin of the peak at 541 nm remains unknown. After 50 ps, the spectrum displays four maxima at 507 nm, 538 nm, 583 nm and 638 nm. This transient spectrum corresponds well to the transient spectrum of the long lived Q_x states (Fig. 9 (c)). This complex dynamical response is understood as the superposition of the responses of uncoupled TPP and SWNTs. Since the electronic relaxation is faster in SWNTs than in TPP, the transient spectrum of the mixture shifts towards the one of TPP over time. The reason why the remaining peaks are narrower than in pristine TPP remains unclear. It may be related to a superposition of the TPP signal onto a slightly shifted negative signal from the nanotubes. In brief, in this configuration, we observe the spectral response of both free porphyrins and SWNTs at 0.2 ps delay and mainly the one of TPP after 50 ps.

In conclusion, pumping at 400 nm results in the excitation of SWNTs and TPP as separate species whereas pumping at 445 nm, in resonance with the Soret band of the SWNT/TPP compound gives rise to transient signatures of predominant SWNT character with a magnified amplitude. These results are in good agreement with a fast excitation transfer from the TPP to SWNTs.

b. S_{22} states dynamics

We investigate the dynamics of the bleaching of the S_{22} transition upon excitation through the Soret band, for a specific probe wavelength (ie, the (6,5) chiral species). The main effect is a drastic increase of amplitude of the transient signal for the compounds (as described in Sec.III B 1), which reflects an effective population creation in the nanotube upon EET from the TPP. However the temporal profiles shown in Figure 11 are almost identical for pristine nanotubes and the compound.

The curve was fitted with $R(t) = A_1 \exp(-t/\tau_1) + A_2 \exp(-t/\tau_2)$. The fitting parameters are reported on the table II.

	A_1	A_2	τ_1	τ_2
SWNT	0.4	0.2	550±50 fs	∼16 ps
SWNT/TPP	0.5	0.2	800 ±20 fs	∼14 ps

TABLE II. Fitting parameters of normalized $\Delta T/T$ dynamics of SWNT and SWNT/TPP, pumped at 445 nm and probed in resonance with S_{22} transition of (6,4) nanotubes.

We note a slight increase of the fast decay time for the compounds compared to pristine SWNTs. The origin of this slight slow-down of the decay, if real, might be related to the transfer dynamics, which again would fall in the 100 fs range. The decay is globally faster than for S_{11} transitions, which is reflected in the larger weight of the fast component. However, this decay remains much slower than the values reported so far the lifetime of S_{22} excitons (less than 100 fs) [22, 34]. Such behavior has been reported in the literature for suspensions of nanotubes and remains unclear. It may be related to nonlinearities (such as Auger processes) in the intrinsic response of nanotubes which couples the dynamics of S_{22} and S_{11} exciton populations [35]. Here we observe this effect for both pristine nanotubes and compounds, which means that the interaction between the chromophore and the tube plays a minor role in this relaxation. However, this possible nonlinear coupling between S_{22} and S_{11} exciton populations prevents us from telling whether the energy is directly transfered from the porphyrin to the S_{22} excitonic levels or whether this bleaching on S_{22} is an indirect effect subsequent to the population buildup on S_{11}.

In total, probing the intermediate states allows to confirm that the excitation is transfered from the TPP to the nanotubes on time-scale shorter than 100 fs. Accord-

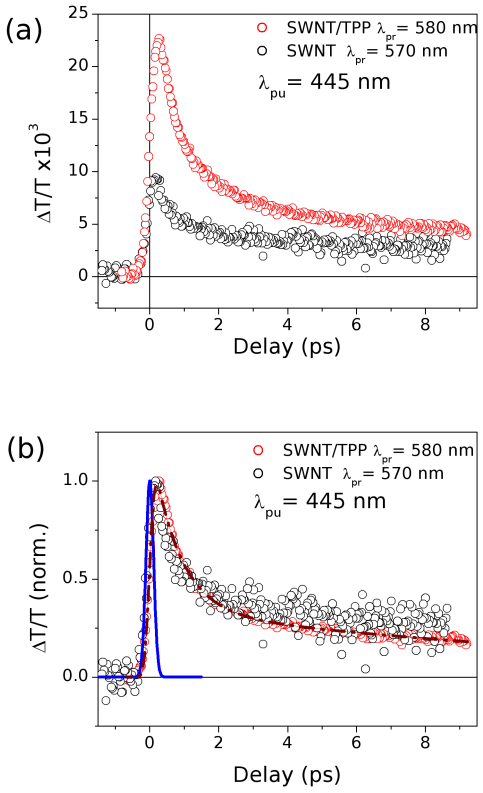

FIG. 11. (a) $\Delta T/T$ dynamics and (b) normalized $\Delta T/T$ of SWNT (black) and SWNT/TPP (red), pumped at 445 nm and probed in resonance with S_{22} transition of (6,5) nanotubes. Dashed line : curve fitting of the SWNT/TPP signal. The pump fluence is 300 μJ/cm^2. Blue line : IRF.

ingly, the transient spectral and dynamical signatures of the compound pumped on the Soret band are those of carbon nanotubes. In contrast, for detuned pumping conditions, both TPP and SWNT participate to the transient response and behave as independent species.

C. Transfer mechanism

Several mechanisms can account for EET. The trivial long range radiative transfer can be rule out since photoluminescence measurements clearly indicate a quenching of the fluorescence of the porphyrins. Accordingly, we checked that a simple mixture of TPP and SWNT micelles without applying the micelle swelling procedure does not display any signature of EET.

It has been established that a fast relaxation to the Q_x states follows the excitation in the Soret band of TPP, on a timescale of less than 100 fs [16]. In the case of TPP/SWNT compounds, the energy transfer occurs on a very similar time scale. If the transfer was to occur directly from the Soret B level to the SWNTs energy levels, the two processes would be in a balanced competition, resulting in a moderate transfer yield. This is in contradiction with the recent estimate of the transfer yield that was consistently measured very close to one (between $1-10^{-3}$ and $1-10^{-5}$) by three independent methods [11]. Therefore, a direct transfer from the B TPP levels can at most account for a small part of the total energy transfer observed in this system. We thus propose that the major part of the energy transfer occurs from the Q_x singlet states of TPP, where the ultrafast transfer can compete efficiently with the relatively long relaxation of TPP ($\sim$12 ns).

The existence of charge separation in nanotube/porphyrins complex has been proposed [7, 8, 36, 37]. In our samples transient absorption spectra show no evidence for the existence of any transient charged species. However, the similarity between our data and the charge transfer dynamics reported for other SWNT based compounds [36], suggests that both processes share common mechanisms. In the case of energy transfer, one can envision the transfer as a simultaneous exchange of an electron and a hole.

Casey et *al.* [10] proposed an electron transfer scheme using redox potentials to order the ground and first excited states of TPP and SWNTs. The redox potential of several nanotubes of identified chiral structure were experimentally determined by several teams in various environments [38–41]. The experimental values agree within a 0.2 V span, which was interpreted as a signature of the different solvatation energies of charged nanotubes in various environment. The redox potential versus the normal hydrogen electrode for small diameter nanotubes (as studied here) turns out to be approximately 0.8 V (valence edge) and -0,3 V (conduction adge). (We note however that the electronic gap deduced from these redox measurements is very close to the optical gap, which is hardly compatible with the large exciton binding energy measured in the same nanotubes. A deeper understanding of many body corrections in redox measurements would be highly desirable but lies beyond the scope of this paper). The redox potential of TPP is 1.2 V. In this hypothesis, the energy levels are ordered as displayed in Fig. 12 (a).

This simple picture allows a basic understanding of the ground and excited states of the compound. In the ground state no charge exchange occurs spontaneously. In contrast, the photo-excitation of the compound results in promoting one electron from the ground state to the B state of the porphyrin. A fast intra molecular relaxation drives this electron to the Q_x Franck-Condon levels, which almost forbids direct EET from B to C_2 states. Electron exchanges can occur from the Q_x state to the C_1 state and from the V_1 state of the SWNT to the ground state of the TPP. This results in the recovery of the TPP molecule and leaves the nanotube in an excited state that will further give rise to NIR luminescence. In this picture, we note that the C_2 and V_2 levels of carbon nanotubes are not directly populated through the transfer process and that no charged species is expected to be produced under illumination.

However, one can argue that the redox potentials reported for SWNTs may be significantly modified once the latter are incorporated in compounds. Furthermore, this electronic description is rather inappropriate for systems where strong Coulomb correlations are known to give rise to excitonic transitions rather than band to band transitions [19]. In this perspective a two-particle (excitonic) description as depicted in Fig. 12 (b) should be more appropriate for describing the observed EET. The energy levels are weakly modified by the coupling between TPP and SWNTs as shown by absorption spectroscopy. The spectral overlap between Q_x and S_{22} bands is expected to give rise to resonant transfer mechanisms.

Non-radiative energy transfer can occur through coulombic interaction as described by Förster theory. This mechanism of interaction has been proposed for EET between carbon nanotubes and organic fluorophores or quantum dots [42, 43] and between nanotubes themselves within small bundles [44, 45]. An extension of this theory beyond the point dipole approximation (i.e. taking into account the one-dimensional character of nanotubes) was recently proposed by Swathi et al. [46] in order to explain EET from an organic emitter to a nanotube. It turns out that the transfer can occur on time scales as short as a few hundreds of femtoseconds for distances below 1 nm. In the Förster theory, the emission band of the donor has to overlap with the absorption band of the acceptor. The TPP PL spectrum shows two relatively narrow peaks at 650 nm and 720 nm. At these wavelengths, SWNTs show S_{22} transitions for some chiral species. Such a Förster mechanism should thus lead to a at least partially selective transfer between TPP and a limited number of SWNTs chiral species. This is rather

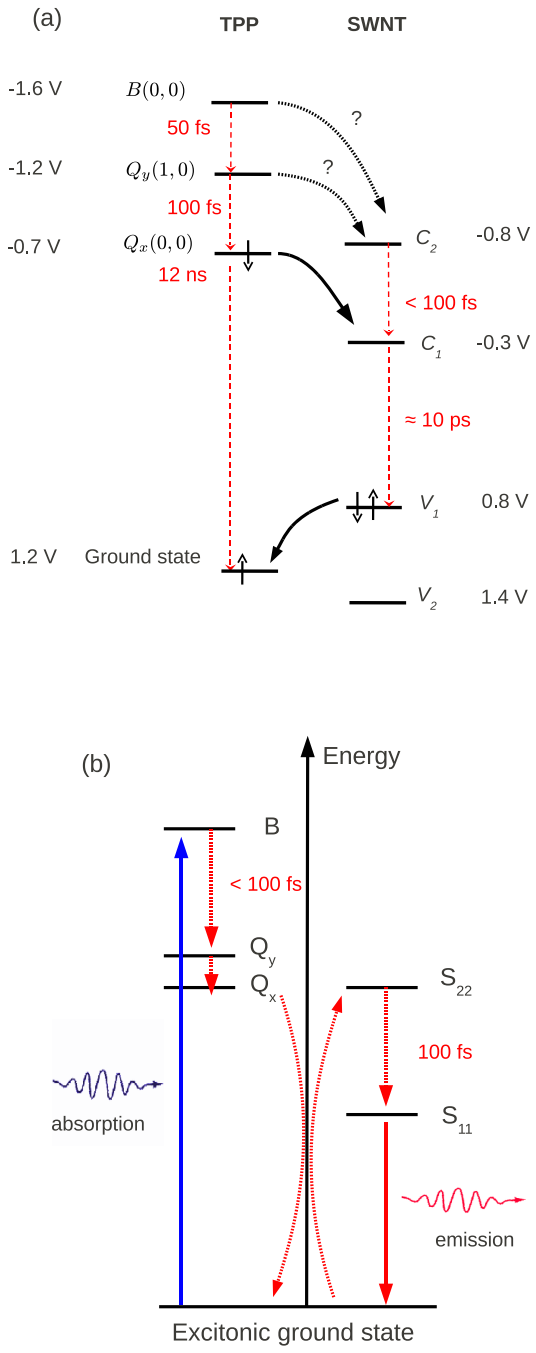

FIG. 12. Schematic model illustrating possible EET mechanisms (a) in an electronic picture through double electron exchange, (b) in an excitonic picture. Values of the redox potential of (6,5) nanotubes are taken from [38–41]. (see text)

in contradiction with the observations reported in section III B 1.

However, the Förster model assumes a long distance interaction between the acceptor and the donor ($\geq$ 10 Å), where direct electron exchange can be neglected. This is hardly compatible with the π-stacking interaction responsible for the stability of the compound. Actually, the red-shift of the resonances of SWNTs in presence of TPP indicate a sizable dielectric screening on the scale of the exciton wave function (which lies in the nanometer range), a length scale where Förster approximation is known to fail. Due to the close vicinity of the donor and the acceptor in SWNT/TPP compound, the porphyrin excited-state wave function can overlap with the excitonic SWNT wave function, such that one should consider electron exchange interactions. This requires a generalized Dexter transfer mechanism. Theoretical investigations are in progress for a deeper description of the mechanism.

IV. CONCLUSION

In conclusion, we have studied the excitation relaxation dynamics in non-covalently bound carbon nanotube/porphyrin compounds. We have established that a fast excitation energy transfer occurs from the porphyrin to the nanotube upon excitation of the Soret band of the former with a characteristic timescale of less than 100 fs. This transfer results in a strongly enhanced ground state recovery dynamics for the porphyrin subunit, whereas an almost instantaneous population buildup is observed on the lowest excitonic level of the nanotube. The global relaxation of the compound is then driven by internal recombination in the nanotube, which occurs on a timescale very close to the one observed in pristine nanotubes. Probing the intermediate states (Q bands and S_{22} bands) allows to confirm that the EET occurs in less than 100 fs. Unfortunately, it does not allow to conclude on whether the S_{22} levels are resonantly populated through the transfer or rather indirectly after the population build-up in the S_{11} levels. Although additional experimental and theoretical investigations are necessary to clarify the transfer mechanism, this study points out the large potentialities of non-covalent compounds involving π-stacking of organic chromophores and nanotubes. These compounds allow both the preservation of the intrinsic properties of the nanotubes but still lead to an efficient enough coupling to the chromophore so to induce new functionalities. The interest of such systems in light-harvesting applications is obvious and forthcoming developments will deal with the use of other chromophores so to cover the entire visible spectrum. Possibly, new chromophore based compounds will show charge transfer paving the way to nanotubes based organic photovoltaic devices.

Acknowledgements

The authors are thankful to P. Plaza and I. Burghardt for helpful discussions. This work was partly funded by grants ANR CEDONA and TRANCHANT and by C'Nano IdF EPONAD.

[1] P. Avouris, Z. Chen, and V. Perebeinos, Nat Nano, **2**, 605 (2007)
[2] C. M. Aguirre, P. L. Levesque, M. Paillet, F. Lapointe, B. C. St-Antoine, P. Desjardins, and R. Martel, Adv. Mater., **21**, 3087 (2009)
[3] S. Berger, F. Iglesias, P. Bonnet, C. Voisin, G. Cassabois, J. S. Lauret, C. Delalande, and P. Roussignol, Journal of Applied Physics, **105**, 094323 (2009)
[4] W. M. Campbell, K. W. Jolley, P. Wagner, K. Wagner, P. J. Walsh, K. C. Gordon, L. Schmidt-Mende, M. K. Nazeeruddin, Q. Wang, M. Grtzel, and D. L. Officer, The Journal of Physical Chemistry C, **111**, 11760 (2007)
[5] D. M. Guldi, Chemical Society Reviews, **31**, 22 (2002)
[6] D. Gust, T. A. Moore, and A. L. Moore, Accounts of Chemical Research, **34**, 40 (2001)
[7] D. M. Guldi, H. Taieb, G. M. A. Rahman, N. Tagmatarchis, and M. Prato, Advanced Materials, **17**, 871 (2005)
[8] G. M. A. Rahman, D. M. Guldi, S. Campidelli, and M. Prato, Journal Of Materials Chemistry, **16**, 62 (2006)
[9] G. Magadur, J. S. Lauret, V. Alain-Rizzo, C. Voisin, P. Roussignol, E. Deleporte, and J. A. Delaire, Chemphyschem, **9**, 1250 (2008)
[10] J. P. Casey, S. M. Bachilo, and R. B. Weisman, Journal of Materials Chemistry, **18**, 1510 (2008)
[11] C. Roquelet, D. Garrot, J. S. Lauret, C. Voisin, V. Alain-Rizzo, P. Roussignol, J. A. Delaire, and E. Deleporte, Applied Physics Letters, **97**, 141918 (2010)
[12] J. Rodriguez and D. Holten, Journal of Chemical Physics, **91**, 3525 (1989)
[13] J. Rodriguez, C. Kirmaier, and D. Holten, Journal of Chemical Physics, **94**, 6020 (1991)
[14] S. Akimoto, T. Yamazaki, I. Yamazaki, and A. Osuka, Chemical Physics Letters, **309**, 177 (1999)
[15] A. Marcelli, P. Foggi, L. Moroni, C. Gellini, and P. R. Salvi, Journal of Physical Chemistry A, **112**, 1864 (2008)
[16] J. S. Baskin, H. Z. Yu, and A. H. Zewail, Journal of Physical Chemistry A, **106**, 9837 (2002)
[17] O. Ohno, Y. Kaizu, and H. Kobayashi, Journal of Chemical Physics, **82**, 1779 (1985)
[18] L. Pekkarinen and H. Linschitz, Journal of the American Chemical Society, **82**, 2407 (1960)
[19] F. Wang, G. Dukovic, L. E. Brus, and T. F. Heinz, Science, **308**, 838 (2005)
[20] J. Maultzsch, R. Pomraenke, S. Reich, E. Chang, D. Prezzi, A. Ruini, E. Molinari, M. S. Strano, C. Thomsen, and C. Lienau, Phys. Rev. B, **72**, 241402 (2005)
[21] C. D. Spataru, S. Ismail-Beigi, L. X. Benedict, and S. G. Louie, Phys. Rev. Lett., **92**, 077402 (2004)
[22] J. S. Lauret, C. Voisin, G. Cassabois, C. Delalande, P. Roussignol, O. Jost, and L. Capes, Physical Review Letters, **90**, 057404 (2003)
[23] F. Wang, G. Dukovic, E. Knoesel, L. E. Brus, and T. F. Heinz, Phys. Rev. B, **70**, 241403 (2004)
[24] Y.-Z. Ma, M. W. Graham, G. R. Fleming, A. A. Green, and M. C. Hersam, Physical Review Letters, **101**, 217402 (2008)
[25] O. J. Korovyanko, C.-X. Sheng, Z. V. Vardeny, A. B. Dalton, and R. H. Baughman, Phys. Rev. Lett., **92**, 017403 (2004)
[26] J. S. Lauret, C. Voisin, S. Berger, G. Cassabois, C. Delalande, P. Roussignol, L. Goux-Capes, and A. Filoramo, Physical Review B, **72** (2005)
[27] S. Berger, C. Voisin, G. Cassabois, C. Delalande, P. Roussignol, and X. Marie, Nano Letters, **7**, 398 (2007)
[28] A. V. Naumov, S. Ghosh, D. A. Tsyboulski, S. M. Bachilo, and R. B. Weisman, ACS Nano, **5**, 1639 (2011)
[29] C. Roquelet, J.-S. Lauret, V. Alain-Rizzo, C. Voisin, R. Fleurier, M. Delarue, D. Garrot, A. Loiseau, P. Rous-

signol, J. A. Delaire, and E. Deleporte, ChemPhysChem, **11**, 1667 (2010)
[30] S. Cambre, W. Wenseleers, J. Culin, S. Van Doorslaer, A. Fonseca, J. B. Nagy, and E. Goovaerts, Chemphyschem, **9**, 1930 (2008)
[31] S. M. Bachilo, M. S. Strano, C. Kittrell, R. H. Hauge, R. E. Smalley, and R. B. Weisman, Science, **298**, 2361 (2002)
[32] S. Berciaud, C. Voisin, H. Yan, B. Chandra, R. Caldwell, Y. Shan, L. E. Brus, J. Hone, and T. F. Heinz, Phys. Rev. B, **81**, 041414 (2010)
[33] S. A. Kovalenko, A. L. Dobryakov, J. Ruthmann, and N. P. Ernsting, Phys. Rev. A, **59**, 2369 (1999)
[34] C. Manzoni, A. Gambetta, E. Menna, M. Meneghetti, G. Lanzani, and G. Cerullo, Phys. Rev. Lett., **94**, 207401 (2005)
[35] Z. Zhu, J. Crochet, M. S. Arnold, M. C. Hersam, H. Ulbricht, D. Resasco, and T. Hertel, The Journal of Physical Chemistry C, **111**, 3831 (2007)
[36] S. D. Stranks, C. Weisspfennig, P. Parkinson, M. B. Johnston, L. M. Herz, and R. J. Nicholas, Nano Letters, **11**, 66 (2011)
[37] S. D. Stranks, J. K. Sprafke, H. L. Anderson, and R. J. Nicholas, ACS Nano, **5**, 2307 (2011)
[38] Y. Tanaka, Y. Hirana, Y. Niidome, K. Kato, S. Saito, and N. Nakashima, Angewandte Chemie International Edition, **48**, 7655 (2009)
[39] A. Nish and R. J. Nicholas, Phys Chem Chem Phys, **8**, 3547 (2006)
[40] M. Zheng and B. A. Diner, Journal of the American Chemical Society, **126**, 15490 (2004)
[41] D. Paolucci, M. M. Franco, M. Iurlo, M. Marcaccio, M. Prato, F. Zerbetto, A. Penicaud, and F. Paolucci, Journal of the American Chemical Society, **130**, 7393 (2008)
[42] A. Ahmad, K. Kern, and K. Balasubramanian, Chemphyschem, **10**, 905 (2009)
[43] V. Biju, T. Itoh, Y. Baba, and M. Ishikawa, Journal of Physical Chemistry B, **110**, 26068 (2006)
[44] P. H. Tan, A. G. Rozhin, T. Hasan, P. Hu, V. Scardaci, W. I. Milne, and A. C. Ferrari, Phys. Rev. Lett., **99**, 137402 (2007)
[45] J. Lefebvre and P. Finnie, The Journal of Physical Chemistry C, **113**, 7536 (2009)
[46] R. S. Swathi and K. L. Sebastian, The Journal of Chemical Physics, **132**, 104502 (2010)

Supplemental Material : Off-resonant excitation

Regarding SWNTs (Fig. 13(a)), the transient spectrum excited at 400 nm shows only slight differences compared to the one excited at 445 nm, essentially in the relative amplitude of the different PB peaks. We explain this observation as due to a change of partially resonant conditions in the excitation (i.e. the energetic distance between the pump and the S_{22} or S_{33} resonances depends on the chiral species resulting in a chiral dependent excitation). In any case, the excitation at 400 nm is more off-resonance than at 445 nm, which explains the overall weaker amplitude of the pump-probe signal in Fig. 13(a) compared to Fig. 9(a).

Figure 13(b) shows the transient transmission spectra of pristine TPP after excitation at 400 nm. The transient spectrum of TPP is very similar to the one obtained after excitation at 445 nm. This means that pumping on either sides of the Soret band of pristine TPP does not affect the relaxation dynamics to the Q bands (which remains on the order of 100 fs as previously reported [16]) nor the branching of the population decay to the different Q levels. Therefore, the transient spectrum of TPP in the visible is mainly due to the transient response of the Franck-Condon levels of the Q_x state that are indifferently populated whatever the excitation wavelength within the Soret band.

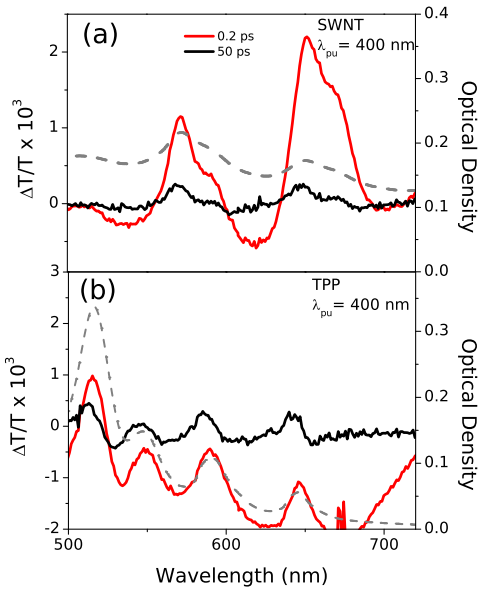

FIG. 13. Transient absorption spectra for SWNT and TPP in SC pumped at 400 nm (a,b) at two different pump-probe delays (0.2 ps (red line) and 50 ps (black line)). The pump fluence is 300 μJ/cm^2. The dashed line is the linear absorption spectrum of the corresponding sample.